Approximation of surfaces with fault(s) and/or rapidly varying data, using a segmentation process, D^m-splines and the finite element method

Running title: **Non Regular Surface Approximation**

Authors: C. Gout[1,2,3], C. Le Guyader[4], L. Romani[5], A.-G. Saint-Guirons[6,3]
Complete affiliations:
[1] : Université de Valenciennes, LAMAV - ISTV2, Le Mont Houy, 59313 Valenciennes Cedex 9, France.
[2] : INSA de Rouen, Laboratoire de Mathématiques de l'INSA, Place Emile Blondel, BP 08, 76 131 Mont-Saint-Aignan Cedex, France.
[3] : INRIA Futurs Research Center Team-Project Magique3D, Pau, France.
[4] : INSA de Rennes, 20 Avenue des Buttes de Coësmes ,CS 14315, 35043 Rennes Cedex, France.
[5] : Università di Milano-Bicocca, Dipartimento di Matematica e Applicazioni, Via R. Cozzi 53, 20125 Milano, Italy.
[6] : Université de Pau et des Pays de l'Adour, Lab. de Math., UMR CNRS 5142 - IPRA, Avenue de l'Université, BP1155, 64018 Pau Cedex, France.
E-mail addresses: chris_gout@cal.berkeley.edu, carole.le-guyader@insa-rennes.fr, lucia.romani@unimib.it, anne-gaelle.saint-guirons@univ-pau.fr

Abstract: In many problems of geophysical interest, one has to deal with data that exhibit complex fault structures. This occurs, for instance, when describing the topography of seafloor surfaces, mountain ranges, volcanoes, islands, or the shape of geological entities, as well as when dealing with reservoir characterization and modelling. In all these circumstances, due to the presence of large and rapid variations in the data, attempting a fitting using conventional approximation methods necessarily leads to instability phenomena or undesirable oscillations which can locally and even globally hinder the approximation. As will be shown in this paper, the right approach to get a good approximant consists, in effect, in applying first a segmentation process to precisely define the locations of large variations and faults, and exploiting then a discrete approximation technique.

To perform the segmentation step, we propose a quasi-automatic algorithm that uses a level set method to obtain from the given (gridded or scattered) Lagrange data several patches delimited by large gradients (or faults). Then, with the knowledge of the location of the discontinuities of the surface, we generate a triangular mesh (which takes into account the identified set of discontinuities) on which a D^m-spline approximant is constructed. To show the efficiency of this technique, we will present the results obtained by its application to synthetic datasets as well as real gridded datasets in Oceanography and Geosciences.

Keywords: Image segmentation, Finite Element Methods, Splines, Surfaces with Faults.

1 Introduction

Description of the topography of seafloor regions (Tonga Trench, Japan Trench, Kermadec Trench, etc.), reservoir characterization in the petroleum industry, volcanology (study of site effects in seismic wave propagation or propagation of pyroclastic flows along the slopes of a volcano), etc... all require the correct reconstruction of non regular surfaces from the knowledge of a given set of surface points. When addressing several geophysical problems, therefore, accomplishing a faithful representation of irregular surfaces by an accurate data fitting process is an issue of great importance, especially when one needs to describe topographic models with high regularity.

Among the existing techniques for surface reconstruction from a set of points, spline methods have become very popular because of their smooth appearance. Nevertheless, in the presence of non regular data, their effectiveness is reduced by overshooting and undershooting near steep gradients. To prevent these oscillations from occurring, many approaches presented in the literature up to now use a non-homogeneous approximant by adding tension to the spline. However, to overcome this issue through the use of weighted splines, B-splines or splines with parameters, it is also required to know the location of the large variations. Franke [20], Nielson and Franke [36], Bouhamidi and Le Méhauté [11] proposed reconstruction techniques that rely on splines under tension without making use of such information, but although they give good results in the case of curve fitting, they do not perform well in the case of surface fitting.

In Apprato and Gout [1] and Gout and Komatitsch [24], the authors presented a successful solution to this kind of bivariate approximation problem that exploits scale transformation families, but the case of

fault is not taken into account.
The main goal of this work is thus to give a quasi-automatic algorithm to determine the location of the large variations and the faults of the surface, in order to use specific methods that rely on splines under tension with a non-constant smoothing parameter ([19], [43]) near the identified set of discontinuities. Likewise, if one wants to use finite element methods ([17]) in the discretization step, it is well known that to correctly reproduce the set of surface discontinuities (both of the function -faults- and/or its derivatives -creases-), there are some constraints regarding the triangulation of the domain of definition of the function: in particular, as shown by Manzanilla [32, p. 114], the edges of the triangles of the triangulation should not intersect the set of discontinuities, here denoted by D (Figure 1).

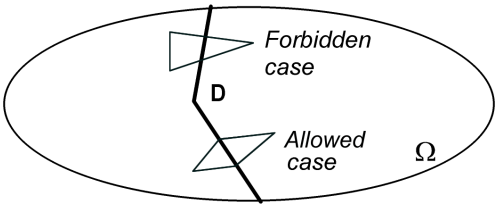

Figure 1: Examples of prohibited and allowed triangles in the domain triangulation: the identified set of discontinuities D must be taken into account.

As a consequence, it is generally necessary to consider a number of different connected open subsets F_i, commonly called patches (Figure 2), and mesh them as done in Figure 3.

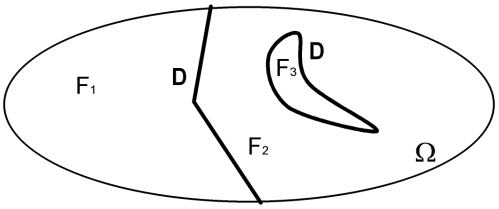

Figure 2: Example of a set of discontinuities D and the three different subsets F_1, F_2, F_3 it delineates.

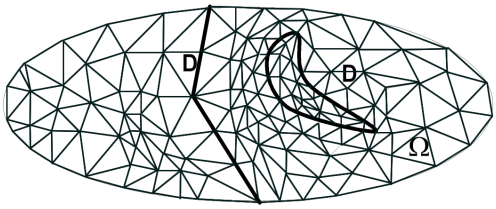

Figure 3: Following the set of discontinuities D in Figure 2, a triangulation is made: no triangle intersects the set of discontinuities (as presented in Figure 1).

Let us note that to improve the results, an *adaptative mesh refinement* can be made near the set D. Then, it would be possible to use a finite element approximant. Unfortunately, because of difficulties linked to the geometry and the number of data points, finite element methods turn out to be hard to use. In this work we will use therefore a D^m-spline approximant ([5]) whose definition takes into account the particular structure of the surface domain, as introduced in [32] and [6]. The algorithm is summarized in Figure 4.

To prepare the reader for the technical section about the D^m-spline approximant construction, we start by fixing some fundamental notations that we will use throughout the paper (Section 2). Then, in Section 3, we introduce the segmentation method that will be exploited to locate the set of discontinuities D of the surface. To that purpose, the input surface is converted into a grayscale image composed of pixels whose brightness values are given by the z-coordinate of the data points on each node of a regular grid. So, it is easy to apply segmentation tools developed in image processing to surface approximation applications. As mentioned in Figure 4, it would be possible to also work with random datasets on a

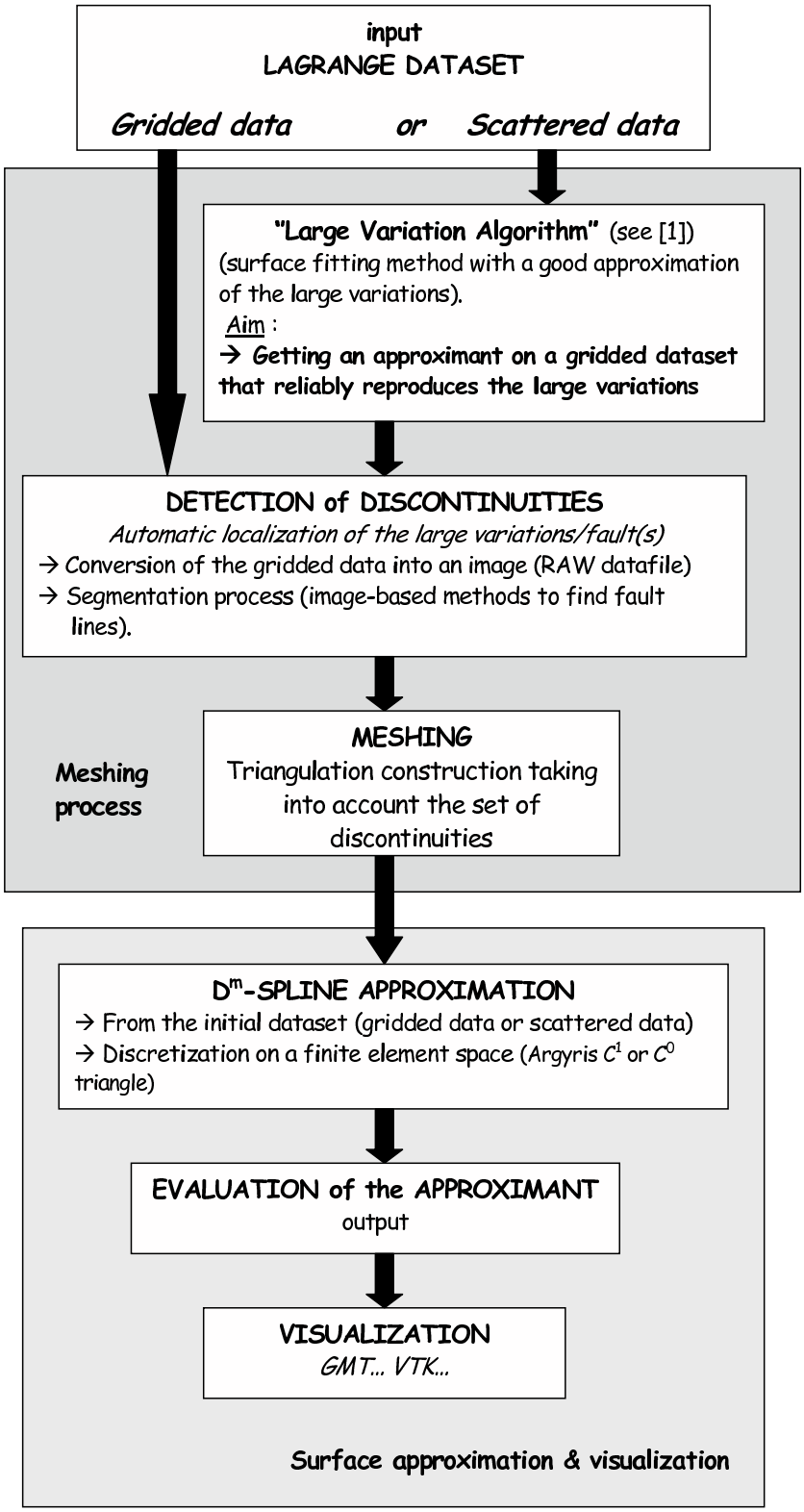

Figure 4: Diagram representing the proposed surface approximation algorithm for gridded or scattered data. In case of gridded data, it is straightforward to get a conversion into an image (*.raw format). Parallel to this, when starting from scattered data, a preprocessing step derived from [1] needs to be applied in order to generate a fairly fine grid dataset suitable for image conversion. Then, taking into account the set of discontinuities identified by the segmentation process, we generate a triangular mesh that is used as the domain of the D^m-spline approximant.

surface, but this paper primarily aims at showing the efficiency of the proposed strategy in the case of regularly distributed points. In Section 4, we then use a finite element method to mesh the surface taking into account the identified set of discontinuities D. The approximation operator is later introduced in the subsequent section and the convergence (see also [1], [7], [8] or [26]) of the method when the number of data tends to infinity is discussed. Numerical results on synthetic datasets and real datasets in Oceanography and Geosciences are given in Section 6.

2 Notations

Let $\mathbb{R}^2$ denote the two dimensional Euclidean space. In the remainder of this paper, for any subset $\Lambda \subset \mathbb{R}^2$, we use $\overline{\Lambda}$, $\partial\Lambda$, $\mathring{\Lambda}$ and $card\ \Lambda$ to refer respectively to the closure, the boundary, the interior and the cardinality of Λ.

Additionally, we assume that Ω is a bounded open set of $\mathbb{R}^2$ and we consider the input dataset constituted by N Lagrange points $(x_i, y_i, z_i)_{i=1,..,N}$, with $(x_i, y_i) \in \Omega$. Denoting by $H^m(., \mathbb{R})$ the classical Sobolev space [17], our goal is thus to determine, from such a finite set of Lagrange data, an approximant $f : \Omega \to \mathbb{R}$ such that $f \in H^m(\Omega', \mathbb{R})$ but $f \notin H^m(\Omega, \mathbb{R})$, where $\Omega' = \Omega \setminus \overline{D}$ and D is a nonempty subset of Ω containing the discontinuities of the surface. This means that we seek an f that is regular on Ω' but not on Ω.

Let us remark that the set Ω' does not have a Lipschitz continuous boundary in the sense of Nečas [35] and, as originally done in [6, p. 647], D can be conveniently represented by a set of connected open subsets $\{F_i\}_{i=1,...,K}$ of Ω (Figure 2) with a Lipschitz continuous boundary satisfying:

$$\begin{cases} (i)\ \forall i, j = 1, ..., K,\ i \neq j,\ F_i \cap F_j = \emptyset, \\ (ii)\ \bigcup_{i=1}^{K} \overline{F}_i = \overline{\Omega}, \\ (iii)\ D \subset \partial F, \text{ where } F = \bigcup_{i=1}^{K} F_i, \\ (iv)\ D \text{ is included in the interior in } \partial F \text{ of } D \cup \partial\Omega, \\ (v)\ \text{the interior in } \partial F \text{ of } \overline{D} \cap \Omega \text{ is included in } D, \\ (vi)\ \overline{D} \cap \partial\Omega \text{ is included in } D. \end{cases} \tag{1}$$

We also define the following spaces (see [49] for more details):

- $C_D^k(\Omega') = \left\{ v \in C^k(\Omega') :\ v_{|F_i} \in C^k(\overline{F}_i)\ \forall i = 1, ..., K \right\}$, where $C^k(\Omega')$ is the space of continuous real-valued functions on Ω' such that all its derivatives of order $\leq k$ are continuous on Ω'. Equipped with the norm $\|v\|_{C_D^k(\Omega')} = \max_{1 \leq i \leq K} \|v\|_{C^k(\overline{F}_i)}$, the space $C_D^k(\Omega')$ is a Banach space (see Manzanilla [32]). Manzanilla also proved [32, Proposition 2.2.1-p.87] that C_D^k and its norm are independent of the choice of the set $\{F_i\}_{i=1,...,K}$.
- $H^k(\Omega')$, the usual Sobolev space.

Using (iii), (iv) and (v) of (1), Arcangéli et al. [6] proved the following non trivial (because Ω' does not have a Lipschitz continuous boundary) topological result:

$$\begin{cases} H^m(\Omega') \hookrightarrow H^k(\Omega') \quad \forall m, k \in \mathbb{N}, m > k, \\ H^m(\Omega') \cap C^k(\overline{\Omega}) \text{ is bounded in } H^m(\Omega') \quad \forall m, k \in \mathbb{N}, m > k + 1. \end{cases}$$

3 Segmentation process

The goal of this section is to introduce a segmentation method to recover the surface patches from the initial surface taking into account its discontinuities.

Let us note that other approaches have been developed: in [40], fault lines are determined using a divergence property of sequences measuring gradients near discontinuities. Parallel to this, recovering functions with discontinuities sampled on a cartesian grid have been studied in [12] and [13]. In [27], Gutzmer and Iske present an algorithm for detecting fault lines from a scattered dataset, which, under reasonable assumptions on the given data, generates polygonal curves approximating the unknown discontinuities. The only user interaction required in the algorithm is the choice of the threshold parameter. Based on a local approximation scheme using thin plate splines combined with a triangulation method, the Gutzmer and Iske algorithm turns out to be stable.

The detection procedure we are proposing in this paper relies on a fast segmentation method. As already pointed out, since the definition of a surface can be strongly linked to that of an image, by associating the height of a surface at a grid node with the brightness value of a pixel at the same location, we can apply segmentation tools for images to surfaces. Due to the fact that a gray-level image is made of pixels which have values between black and white, surface areas corresponding to large variations or faults in the data, will be identified by a dark zone in front of a clear one. In this way, the set of discontinuities D will be easily determined by an image segmentation method.
In the last two decades, many strategies have been proposed in the literature for segmenting images.
The level set method introduced by Osher and Sethian [37] (see also Osher and Fedkiw [38], Sethian [48] and [30], [31]) is a very popular way for dealing with such a problem. It is based on a curve evolution approach that consists in considering the evolving curve as the zero level set of a surface. This modelling makes it possible to naturally handle topological changes when the surface is evolving, and since the evolution of the curve only depends on geometric features such as curvature and normal vector, it turns out to be also easy to implement.

The geodesic active contour model [15], a typical boundary-based level set method, has been widely used in image segmentation and extended to medical and geophysical imaging too. It usually depends on local features of the image such as gradients, which make the technique very sensitive to noise. In addition, the method does not work well when the contrast of the image is impaired since, in this case, the evolving curve does not stop its evolution. Therefore, it results in an inaccurate segmentation of the object.

Chan and Vese [50] proposed a new model for active contours to detect objects in a given image, based on techniques of curve evolution and level sets. Their model is a particular case of the minimal partition problem which derives from the Mumford-Shah functional for segmentation. Contrary to classical methods which involve a stopping criterion based on the gradients of the image, this method takes into account the information contained in the regions delineated by the evolving contour and allows the detection of objects which are not necessarily defined through their gradients. However, it does not perform satisfactorily to extract certain structures or regions from images with complicated background. Some researchers attempted to integrate boundary and region information within the same framework, like the Geodesic Active Region model (see [16], [39], [42], [44]). In order to achieve better segmentation results, some kind of external forces were added to the level set method.

To improve the accuracy of this process, another possibility could be to use a segmentation model integrating geometrical constraints while satisfying the classical criteria of detection (with in particular the regularity needed on the contour (see [25], [28] or [23] for more details)). Fitting the model on geometrical data increases the process accuracy. The idea that governs this strategy consists in seeking a geodesic curve in a Riemann space whose metric depends both on the image contents and on the geometrical constraints (see [23] for more details).

In this work we propose to use an approach based on the geodesic active contour method. We recall that its general formulation corresponds to the following PDE:

$$\frac{\partial \mathcal{C}}{\partial t}(q,t) = \mathcal{F}(t,\kappa,\kappa',q)\overrightarrow{n}(q,t), \tag{2}$$

where $\mathcal{F}$ is the speed function, κ is the curvature and κ' its derivative, t is the time variable and $\overrightarrow{n}$ the (inward) normal vector to the curve $\mathcal{C}$ at point $\mathcal{C}(q,t)$.

In our case, we define the speed function as:

$$\mathcal{F} = c_1 g\kappa + c_2\left(-\triangle\left(\mathcal{G}_\nu * \mathcal{I}\right)\right) - c_3 g,$$

where $c_1, c_2, c_3 > 0$, $\mathcal{G}_\nu * \mathcal{I}$ is the smoothed intensity function obtained by convoluting the image with a Gaussian filter of variance ν. The function g is data-dependent, monotone non-increasing and nonnegative and g stops the deformation of the evolving contour when reaching the object boundary. A classical choice to define g is:

$$g(\mathcal{C}) = \frac{1}{1+\left|\nabla\left(\mathcal{G}_\nu * \mathcal{I}(\mathcal{C})\right)\right|^2}.$$

In the numerical section of this paper, we have taken: $c_1 = 0.15$, $c_2 = 0.1$, $c_3 = 1$.

An explicit Lagrangian approach can be used to simulate (2). In this case, the topology and geometry of the model are explicitly represented during the simulation of the contour flow. The evolution process can be basically approximated by:

$$\mathcal{C}(q,t+\Delta t) = \mathcal{C}(q,t) + \Delta t\mathcal{F}(t,\kappa,q)\overrightarrow{n}.$$

In this work we use a level set approach to simulate the contour flow. The level set method (Osher and Sethian [37], see also [38], [48]) allows the evolving front to change topology, break and merge, which means that it can extract the boundaries of particularly intricate contours. In this technique the contour is initialized inside the desired region and grows.

4 Mesh generation

As explained in [32] and [6], the key point of the mesh generation step consists in taking into account the set D when making the triangulation. To this aim, let $\mathcal{H}$ be a bounded subset in $\mathbb{R}_+^*$ for which 0 is an accumulation point, and, for any $h \in \mathcal{H}$, let $\mathcal{T}_h$ be a triangulation on $\overline{\Omega}$ by means of triangle elements T whose diameters h_T are $\leq h$, such that

$$\forall T \in \mathcal{T}_h,\ \overset{\circ}{T} \cap D = \emptyset, \tag{3}$$

and

$$\begin{cases} \text{each side of a triangle } T \in \mathcal{T}_h \text{ is either a side of another} \\ \text{triangle } T \in \mathcal{T}_h, \text{ or a part of } \partial\Omega, \text{ or a part of } D, \end{cases} \tag{4}$$

as shown in Figures 1 and 3. It is clear that the family $(\Omega_h)_{h\in\mathcal{H}}$, made of all the subsets defined by the interior of the union of all triangles T of $\mathcal{T}_h$, satisfies the relations $\Omega \subset \Omega_h\ \forall h \in \mathcal{H}$ and $\lim_{h\to 0} meas(\Omega_h \backslash \overline{\Omega}) = 0$.

Additionally, let us note that to satisfy the hypothesis (3), one needs to either use isoparametric finite elements (triangles with a curved side to fit the set of discontinuities obtained after the segmentation process), or approximate the segmentation curve in order to obtain a set of discontinuities with a polygonal boundary that allows to use usual finite elements (Argyris, Bell, Hsieh-Clough-Tocher or Powell-Sabin triangles). For any $h \in \mathcal{H}$, we define by V_h the finite element space constructed on $\mathcal{T}_h$, such that

$$\begin{cases} V_h \text{ is a finite-dimensional subspace} \\ \text{of } H^m(\Omega') \cap C_D^k(\Omega'). \end{cases} \tag{5}$$

Let us note that if the space V_h is defined as in (5), the definition of the function belonging to V_h can represent vertical faults. But to represent creases (discontinuities of the derivatives), it is necessary to use a finite dimensional subspace of $H^m(\Omega') \cap C_D^k(\Omega') \cap C^0(\overline{\Omega})$. In real problems, we usually take $k = 1$ or 2 and $m = 2$.

When $m = 2$, we could use for example:
- the finite element of class C^1: Argyris, Bell, Hsieh-Clough-Tocher or Powell-Sabin triangle [17];
- the finite element of class C^2: Argyris, Bell, Hsieh-Clough-Tocher or Powell-Sabin triangle [51].

When $m = 3$, we could use the C^2 finite element introduced when $m = 2$. Likewise, to take into account the discontinuities of the function, we are going to split into two parts the degrees of freedom of the nodes of the triangulation located on D. Each of them is only linked to the finite element located on the same side of D. For more details about this method, the reader is referred to [32, Remark 2.6.1, p. 120].

There is a number of public domain triangular mesh generators. A complete list of them can be seen on the web pages:
http://www-users.informatik.rwth-aachen.de/~roberts/software.html
and http://www.andrew.cmu.edu/user/sowen/software/triangle.html.
Among these, we recall a few tools that can be used to perform the meshing step in our algorithm:

- GAMMA software (INRIA) [21], which includes the following 2D mesh generators:
  * Bamg: Bidimensional Anisotropic Mesh Generator.
  * BL2D-V2: plane isotropic or anisotropic mesh generator.
  * EMC2: wysiwyg 2D finite elements mesh generator.
- Mefisto software (Alain Perronnet) [33]: Structured or non-structured generation of 2D and 3D meshes, part of the Mefisto finite element program.
- METIS (Karypis Lab) [34]: A C program which can partition a graph, partition a finite element mesh, or reorder a sparse matrix.

5 Approximation operator

5.1 Discrete smoothing D^m-spline on Ω'

We keep the notations previously introduced. We also define a finite subset A of N distinct points of $\overline{\Omega}$ and a linear mapping $\rho : C_D^0(\Omega') \to \mathbb{R}^N$ such that

$$\rho(v) = v(a) \in \mathbb{R}^N$$

with $a = (a_1, ..., a_N) \in A \backslash D$. We then introduce the following functional:

$$\forall \varepsilon > 0, \forall \beta \in \mathbb{R}^N, \forall v \in H^m(\Omega'),\ J_\varepsilon(v) = \langle \rho v - \beta \rangle_{\mathbb{R}^N}^2 + \varepsilon |v|_{m,\Omega'}^2, \tag{6}$$

where β corresponds to the vector of the z-values of the wanted surface (that is $\beta = (z_i)_{1 \le i \le N}$), $\langle \cdot \rangle_{\mathbb{R}^N}$ is the euclidean norm in $\mathbb{R}^N$ and $|.|$ is the semi-norm $|v|_{m,\Omega'} = (v,v)_{m,\Omega'}^{\frac{1}{2}}$.

We recall (see Arcangéli [5], Arcangéli et al. [6] and [7], [32], [2], [3], [4], see also [47] for penalized least squares fitting method) that the smoothing D^m-spline is the solution of the following minimization problem: find σ_ε such that

$$\begin{cases} \sigma_\varepsilon \in H^m(\Omega'), \\ \forall v \in H^m(\Omega'),\ J_\varepsilon(\sigma_\varepsilon) \le J_\varepsilon(v), \end{cases}$$

which is equivalent to the following one:

$$\begin{cases} \sigma_\varepsilon \in H^m(\Omega'), \\ \forall v \in H^m(\Omega'),\ \langle \rho\sigma_\varepsilon, \rho v \rangle_{\mathbb{R}^N} + \varepsilon (\sigma_\varepsilon, v)_{m,\Omega'} = \langle \beta, \rho v \rangle_{\mathbb{R}^N}. \end{cases}$$

Arcangéli et al. [6] established the existence and uniqueness of the solution of this minimization problem (using Lax-Milgram lemma). This solution is the smoothing D^m-spline related to β, Ω', and ε.

Remark: We recall that we take into account the discontinuities of the function in the discretization, when we split into two parts the degrees of freedom of nodes of the triangulation located on D.

We then give the definition of the discrete smoothing D^m-spline. In order to compute a discrete approximant, we could use a Bézier-polynomial space or any other finite dimensional space ([10], [29], [46], [9]). We choose here a finite element representation of the discrete approximant, which enables us to obtain a very small sparse linear system and an easier study of the convergence of the approximation. So, $\forall \varepsilon > 0, \forall \beta \in \mathbb{R}^N, \forall h \in \mathcal{H}$, we consider the following problem: find $\sigma_{\varepsilon,h}$ satisfying

$$\begin{cases} \sigma_{\varepsilon,h} \in V_h, \\ \forall v_h \in V_h,\ J_\varepsilon(\sigma_{\varepsilon,h}) \le J_\varepsilon(v_h), \end{cases} \tag{7}$$

where J_ε is the functional introduced in (6) and V_h the space defined in (5). Using Lax-Milgram lemma, we can show that this problem has a unique solution $\sigma_{\varepsilon,h}$.

Denoting by $M = M(h)$ the dimension of V_h and by $\{\varsigma_j\}_{1 \le j \le M}$ one basis of V_h, we set

$$\sigma_{\varepsilon,h} = \sum_{j=1}^{M} \alpha_j \varsigma_j,$$

with $\alpha_j \in \mathbb{R}, 1 \le j \le M$.
Introducing the matrices $P = \{p_{ij}\}_{1 \le i \le N, 1 \le j \le M}$ and $Q = \{q_{ij}\}_{1 \le i,j \le M}$ with $p_{ij} = (\varsigma_j(a_i))_{1 \le i \le N, 1 \le j \le M}$ and $q_{ij} = (\varsigma_i, \varsigma_j)_{m,\Omega_h}$, we see that (7) is equivalent to the problem:

$$\begin{cases} find\ \alpha = (\alpha_1, ..., \alpha_i, ..., \alpha_M)^t \in \mathbb{R}^M\ solution\ of \\ (P^tP + \varepsilon Q)\,\alpha = P^t\beta. \end{cases}$$

We remark that the matrix $(P^tP + \varepsilon Q)$ is symmetric and positive definite of dimension $M \times M$. Since the smoothing parameter ε is data-dependent, its value should be opportunely chosen for each dataset. As concerns the examples in Section 6, we have taken $\varepsilon = 10^{-6}$. Cross-validation methods to test the choice of ε when dealing with similar penalized least-squares problems can be found in Deshpande and Girard [18] and Girard [22].

5.2 Rapidly varying data algorithm

After the segmentation process, the main discontinuities of the (gridded or scattered) dataset have been found, but in other part(s), rapidly varying data may still exist. In order to take into account this fact, we propose to use a specific method introduced in Apprato and Gout [1].

This method uses two scale transformations, namely φ_d for the pre-processing and ψ_d for the post-processing, in order to suppress or at least dampen the oscillations of the approximation near such locations. The first one, φ_d, is used to transform the z-values representing the height of the unknown surface f into values $\{u_i\}_{1\leq i\leq N}$, regularly distributed in an interval chosen by the user. The pre-processing function φ_d is such that the transformed data do not present large variations, and therefore, the spline operator σ_ε^d can subsequently be applied without generating significant oscillations. The second scale transformation ψ_d is then applied to the approximated values to map them back and obtain the approximated values of z. It is important to underline that the proposed scale transformations do not create parasitic oscillations. Moreover, this method is applied without any particular knowledge of the location of the large variations in the dataset.

Let us consider a dataset $\left(x_i^d, y_i^d, z_i^d\right)_{i=1,..,N(d)}$ indexed with the real d, such that when d tends to 0, the number of data points $N(d)$ tends to infinity. With the purpose of a theoretical study of the convergence of the approximation, we introduce a function $f : \Omega' \longrightarrow [a, b]$, $f \in H^m(\Omega')$, such that the dataset becomes $\left(x_i^d, y_i^d, z_i^d = f(x_i^d, y_i^d)\right)_{i=1,..,N(d)}$. The functions introduced above have the following expressions for $m \in \mathbb{N}$:

- $\varphi_d : [a, b] \to [a', b'] \subset \mathbb{R}$,
- $\sigma_\varepsilon^d : (\varphi_d \circ f) \in H^m(\Omega', [a', b']) \to \sigma_\varepsilon^d(\varphi_d \circ f) \in H^m(\Omega', [a', b'])$,
- $\psi_d \circ \left(\sigma_\varepsilon^d(\varphi_d \circ f)\right) \in H^m(\Omega', [a, b])$,

where the pre-processing φ_d and the post-processing ψ_d are scale transformation families and where σ_ε^d is an approximation operator, for instance a spline.

We also consider a finite subset A^d of $N(d)$ distinct points of Ω' such that

$$\sup_{(x,y)\in\overline{\Omega'}} \delta\left((x, y), A^d\right) = d, \tag{8}$$

where δ is the Euclidean distance of $\mathbb{R}^2$; the index d represents the radius of the biggest sphere included in Ω' that does not intersect any point of A^d, and thus, when d tends to 0, the number of data points tends to infinity. We also introduce the set Z_1^d of $N(d)$ reals such that

$$\forall (x_i^d, y_i^d) \in A^d, \quad f(x_i^d, y_i^d) \in Z_1^d, \tag{9}$$

and the sequence Z_2^d of $p(d)$ distinct z-values obtained from the ordering of Z_1^d as it follows: $\forall \widetilde{z}_i^d \in Z_2^d, i = 1, ..., p(d)$,

$$a = \widetilde{z}_1^d < \widetilde{z}_2^d < \widetilde{z}_3^d < ... < \widetilde{z}_{p(d)-1}^d < \widetilde{z}_{p(d)}^d = b, \tag{10}$$

where $[a, b] = \mathrm{Im}(f)$. The sequence Z_2^d will be used for the construction of the scale transformation families in the next section. In what follows, we also write for convenience (z_i) instead of $\left(\widetilde{z}_i^d\right)$.

To construct the functions (φ_d) and (ψ_d), we refer the reader to [1] and [24] (see also Torrens [49]). Other constructions based on splines under tension or B-splines are also possible ([14], [41], [45]).

5.3 Convergence of the approximation operator

We first give the convergence of the D^m-spline operator σ_ε^d related to the transformed data $(\varphi_d \circ f)$ to the function $\varphi \circ f$ when d tends to 0. We obtain this result using the convergence of φ_d to φ, knowing that in [5] it was shown that $\lim_{d\to 0} \sigma_\varepsilon^d(g) = g$, for any function g.

Keeping the notations of the previous sections, and as $(\varphi_d \circ f)$ is bounded in $C^m\left(\overline{\Omega'}\right)$, in [1] it was proved that

$$\lim_{d\to 0} \left(\sigma_\varepsilon^d(\varphi_d \circ f)\right) = \varphi \circ f \ \text{ in } \ C^0\left(\overline{\Omega'}\right). \tag{11}$$

From this relation, using a compactness argument, in [1] the authors established a theoretical result concerning the convergence of the approximation (ψ_d converging to φ^{-1} by construction):

$$\lim_{d\to 0} \left\{\psi_d \circ \sigma_\varepsilon^d(\varphi_d \circ f)\right\} = \varphi^{-1} \circ \varphi \circ f = f \text{ in } \ H^{m-\theta}(\Omega'), \tag{12}$$

for any $\theta > 0$ such that $\theta < m - 1$.

We also have the following convergence theorem (in the related proof we use norm equivalence and compactness arguments):

Theorem. *Let $\mathcal{D}$ be a bounded subset in $\mathbb{R}_+^*$ for which 0 is an accumulation point. Then, under the hypothesis*

$$\exists C > 0 : \forall d \in \mathcal{D}, \forall h \in \mathcal{H}, \forall T \in \mathcal{T}_h,\ card(A^d \cap T) \leq C\frac{h^2}{d^2}$$

we have:

$$\lim_{d \to 0} \left\| \psi_d \circ \sigma_{\epsilon,h}^d(\varphi_d \circ f) - f \right\|_{m,\Omega'} = 0,$$

where $\sigma_{\epsilon,h}^d(\varphi_d \circ f)$ corresponds to the D^m-spline $\sigma_{\varepsilon,h}$ introduced in (7) but applied on the pre-processed data $(\varphi_d \circ f)$ and indexed by the real d.

6 Numerical examples

In this section we start by giving an example of surface approximation from scattered and gridded data sampled on an explicit function with fault. We then show the efficiency of the proposed technique applying it firstly to rapidly varying data corresponding to the seafloor surface of one of the deepest parts of the Tonga Trench (Pacific Ocean) and successively to a geological surface with fault situated in the Vallee d'Ossau, Pyrenees mountains (France).
These experiments have been performed on a 2.00 GHz Intel Core 2 Duo Processor T72000 with 2.00 GB of RAM. CPU time: the segmentation process takes less than 3 seconds for each example, the spline approximation takes between 3.3 seconds (subsection 6.1) and 12.2 seconds (subsection 6.3).

6.1 Explicit function with fault

Let $\Omega = [0,1]\times[0,1]$ and let $(0.,0.2), (0.2,0.2), (0.35,0.225)$, $(0.42,0.3), (0.48,0.4), (0.49,0.53), (0.5,0.65), (0.65,0.725), (0.8,0.75), (1.,0.8)$ be the nodes of a polygonal curve identifying a fault D on Ω.
In this first example we start by considering a scattered datafile made of 1500 points irregularly distributed in the domain Ω (see Figure 5).

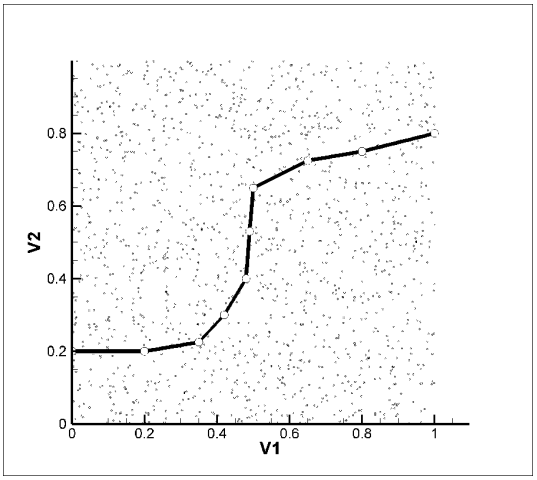

Figure 5: 2D view of the scattered dataset (1500 points) and the fault.

Due to the presence of D, Ω turns out to be divided into two zones. We denote by ω the part of Ω located above the fault (according to the y-axis direction). We then consider the explicit function f:

$$f(x,y) = \frac{1}{\left(\left(3x - \frac{7}{2}\right)^2 + \left(3y - \frac{7}{2}\right)^2\right)} + g(x,y)$$

where

$$g(x,y) = \begin{cases} 0.35 + \exp\left(-\left(3x - \frac{3}{2}\right)^2 - \left(3y - \frac{3}{2}\right)^2\right) \text{ if } (x,y) \in \omega \\ 0 \text{ if not.} \end{cases}$$

In Figures 6 and 7 we give respectively a 3D view of the exact function f and the considered scattered dataset containing the fault.
Since to perform the segmentation step aiming at automatically localizing the fault contained in the dataset it is required to convert it into an image, we will apply the Large Variation Algorithm originally proposed in [1] on a triangulation made of 100 triangles, assuming V_h to be the Argyris finite element space of class C^1.

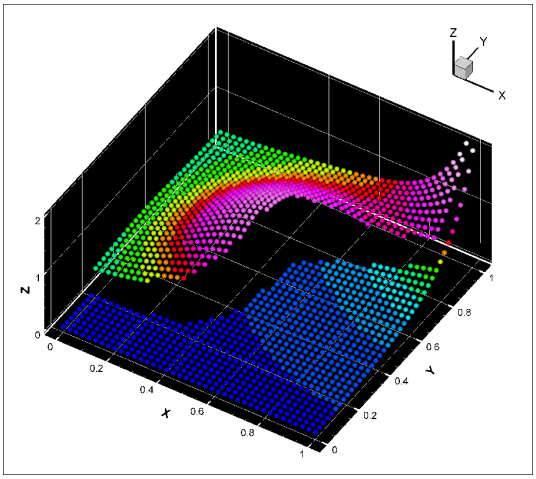

Figure 6: 3D view of the exact function with the fault.

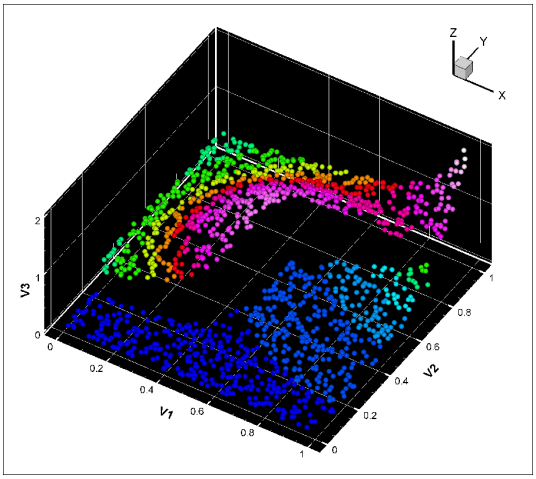

Figure 7: 3D view of the scattered dataset (1500 data points) containing the fault.

Then, evaluating the resulting approximant on a 300×300 regular grid, we get the surface in Figure 8 (left). Of course, the obtained surface is regular, but the crucial point is that the accomplished fitting ensures an excellent general agreement between the constructed large variation and the original discontinuity. Therefore, if we proceed by applying the proposed segmentation process to locate the large variation of this approximant, we get a correct identification of the fault, in particular in the zone where the height difference is the largest one (see Figure 8 (right)). Although the fault line reconstruction is not perfect, the mesh we get from the segmentation step will certainly be much more accurate than any other "blind" mesh.

In Figure 9 we show the approximant we obtained using a meshing of 100 triangles where V_h is assumed to be the Argyris finite element space of class C^1. The quadratic error on the 1500 data points turns out to be equal to 0.00276, while it is equal to 0.0785 using a usual D^m-spline.

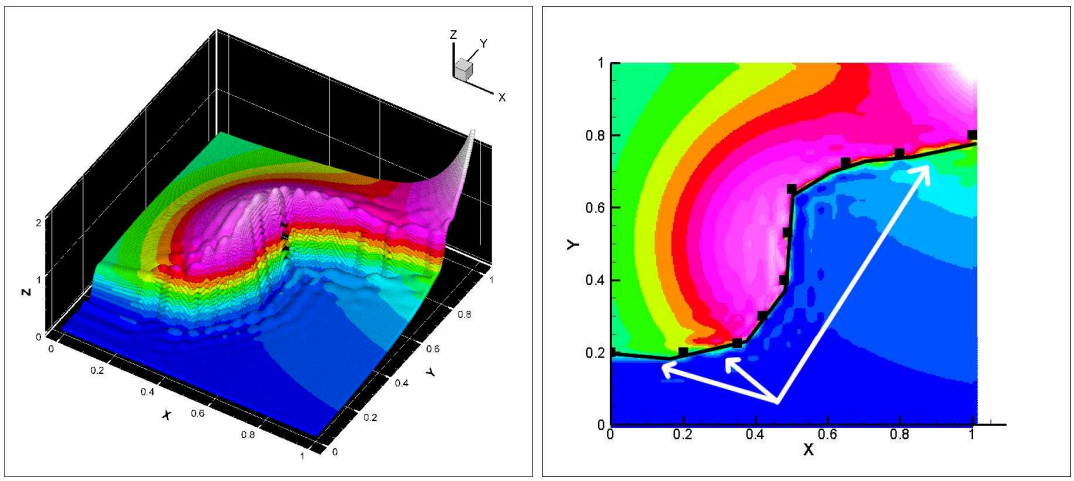

Figure 8: Left: Large Variation Algorithm applied to the scattered dataset in Figure 7 to construct a regular approximant that sampled on a grid allows a straightforward conversion to an image (*.raw format). Right: 2D view of the obtained surface. The polygonal curve represents the result of the segmentation process. In this image, we have also included the nodes identifying the fault D. The white arrows show some zones where there is a little difference between the segmented curve and the original fault. Note how, in other zones, the segmentation process has correctly determined the location of the fault.

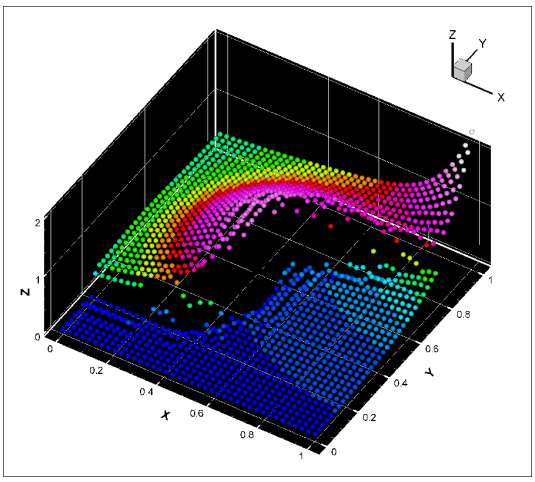

Figure 9: Approximation from the scattered dataset. We can see that the approximant is globally close to the exact function in Figure 6.

To illustrate the method for gridded data, we now consider a gridded datafile of 1600 points sampled from the same function f. Starting from this gridded dataset, we can directly find the fault performing the segmentation process (Figure 10).

In this case, the set of discontinuities is perfectly determined. A 3D view of the resulting approximant computed on a triangulation of 100 triangles where V_h is the Argyris finite element space of class C^1, is given in Figure 11. As it appears, no oscillations are present and the obtained surface is very close to the exact function.

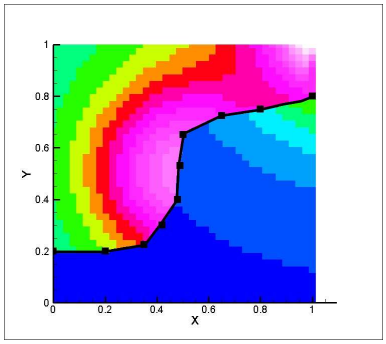

Figure 10: 2D view of the gridded dataset and the fault obtained by applying the segmentation process on the gridded points. In comparison with the scattered data case, the fault is perfectly determined everywhere.

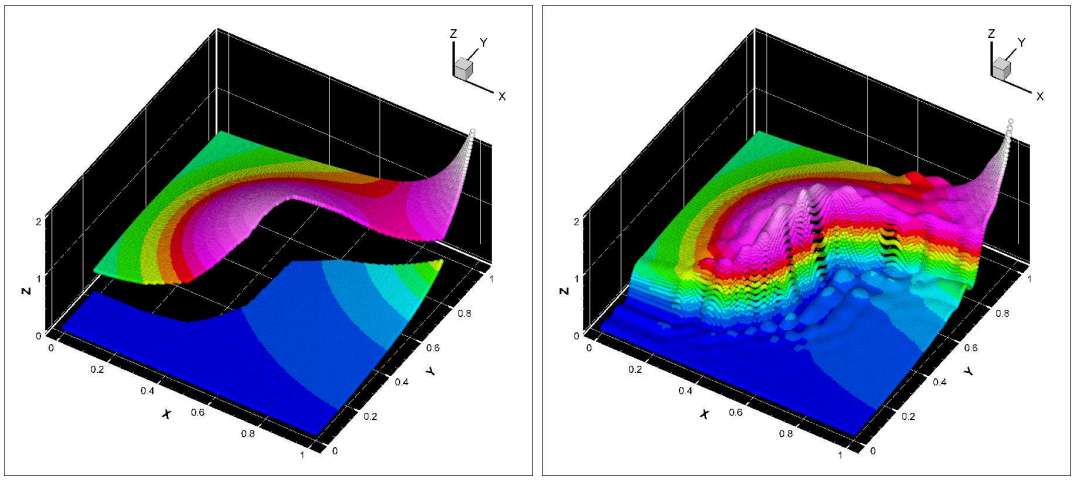

Figure 11: Left: 3D view of the locally C^1 approximant obtained from the considered gridded dataset using the algorithm of Figure 4. The fault contained in the data is clearly determined. Right: 3D view of the C^1 approximant obtained from the same gridded datafile using a usual D^m-spline. The resulting surface is continuous and it additionnally shows some parasitic oscillations.

6.2 Geological surface with rapidly varying data

The Tonga Trench is located in the Pacific Ocean and is 10,882 meter (35,702 ft) deep at its deepest point, known as Horizon Deep (Figure 13). The trench and its arc form an active subduction zone between two plates of the lithosphere, the Pacific Plate being subducted below the Tonga Plate at the northeastern corner of the Australian Plate. The Tonga Trench spreads in the north-northeast of the Kermadec Islands which are situated in the northeast of New Zealand's North Island (Figure 12).

The trench turns west north of the Tonga Plate and becomes a transform fault zone. The convergence is taking place at a rate estimated at approximately 15 centimeters (6 in) per year; however, recent Global Positioning Satellite measurements indicate in places a convergence of 24 centimeters (10 in) per year across the northern Tonga Trench, which is the fastest plate velocity recorded on the planet. Such oceanic trenches are important sites for the formation of what will become continental crust and for the recycling of material back into the mantle. Along the Tonga Trench, mantle-derived melts are transferred to the island arc systems, and abyssal oceanic sediments and fragments of oceanic crust are collected. The Kermadec Trench, to the south, is basically an extension of the Tonga Trench. This zone presents large variations and is of great interest to study. In our example we focus on the deepest part of the Tonga Trench. The considered dataset is made of 8113 points distributed on a (61 $\times$133, *source: USGS*) regular grid. Applying the segmentation method presented in Section 3, the rapid variations contained in the data are localized and three patches are hence identified (Figure 14).

Then, following the patches configuration, a triangulation is made and a D^m-spline approximation is performed.

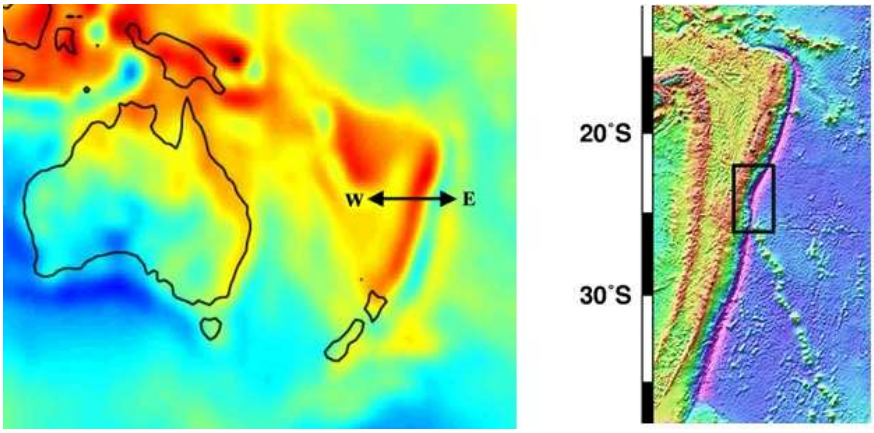

Figure 12: Regional location map of the studied area. Left: Tonga Trench is located north-northeast of New Zealand. Right: Studied area is marked by a box. It corresponds to one of the deepest zones of the Tonga Trench. *Source: U. Texas at Austin and UC San Diego.*

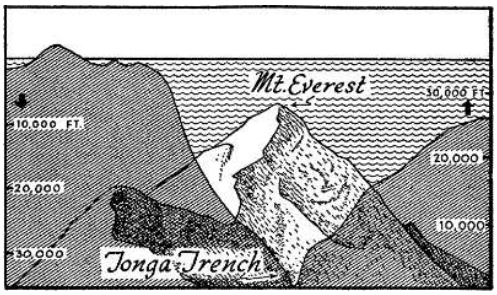

Figure 13: Tonga Trench is deeper than Everest in high (35,702 ft vs 29,029 ft). *Source: Norton, Exploring the deep Pacific, NY.*

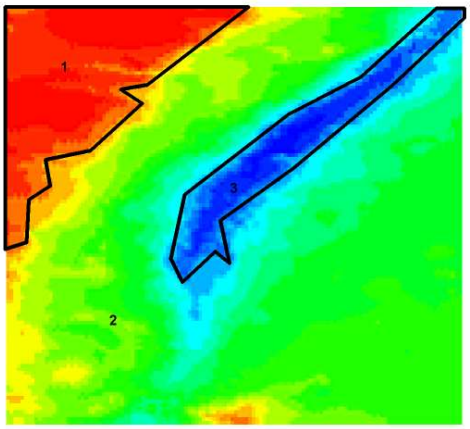

Figure 14: South Tonga Trench, grid of 8113 data points, after the segmentation process (applied twice to get two patches, with a polygonal approximation of their boundary).

Here are the parameters used when running the proposed algorithm on this first real world example:
- the triangulation is made using 325 triangles;
- the finite element adopted is the Argyris triangle (class C^1);
- the smoothing parameter ϵ is chosen equal to 10^{-6};
- the evaluation grid is 200×200.

The quadratic error on the 8113 data points turns out to be equal to $4.782\ 10^{-4}$. This is a very good result. No spurious oscillations are present near the rapidly varying data, as it appears by comparing Figure 16 with Figure 17. A 2D visualization of the obtained surface can be seen in Figure 15. In Figure

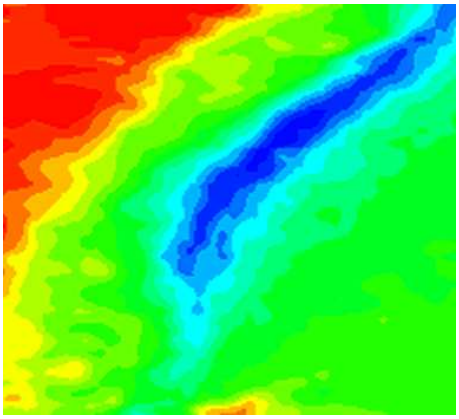

Figure 15: 2D view of the South Tonga Trench approximant.

18, we also give the contour plots of the dataset and the C^1 approximant with isolines.

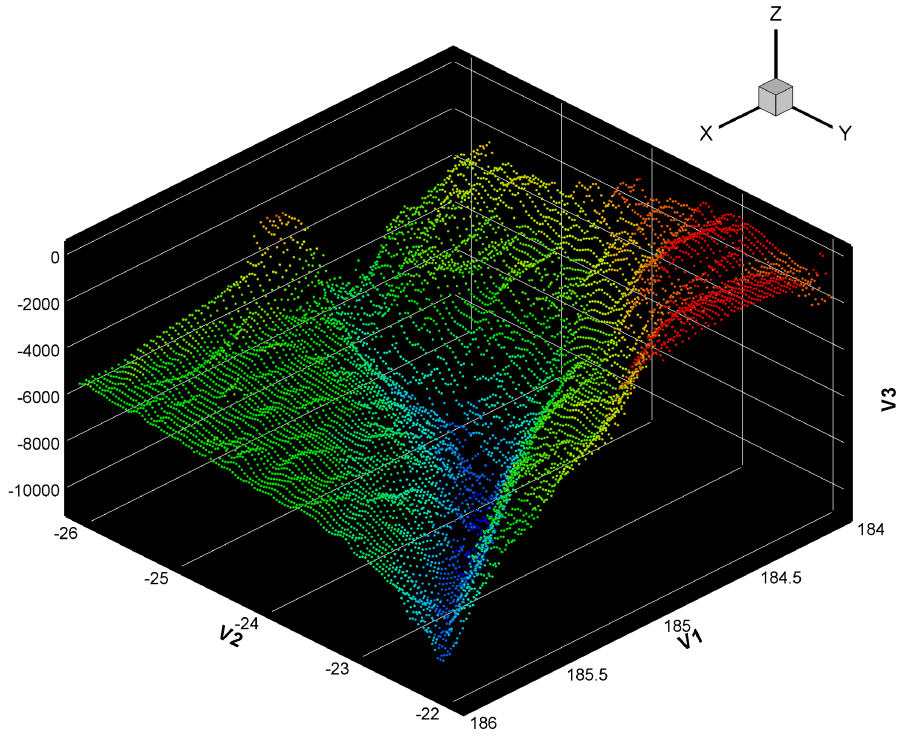

Figure 16: 3D view of the South Tonga Trench dataset (8113 data points).

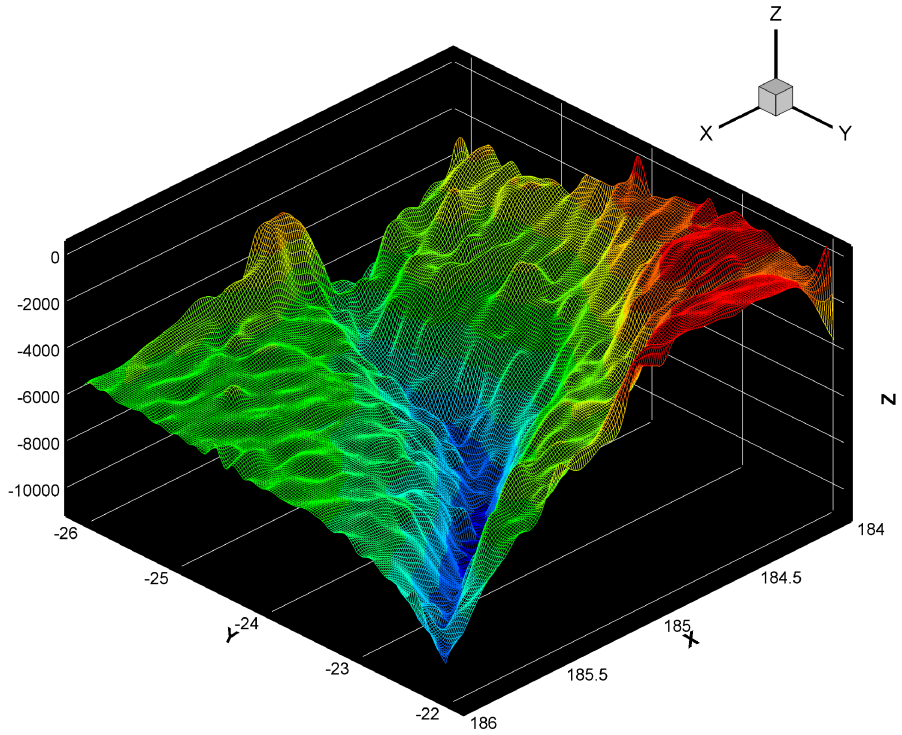

Figure 17: 3D view of the C^1 approximant of the South Tonga Trench dataset.

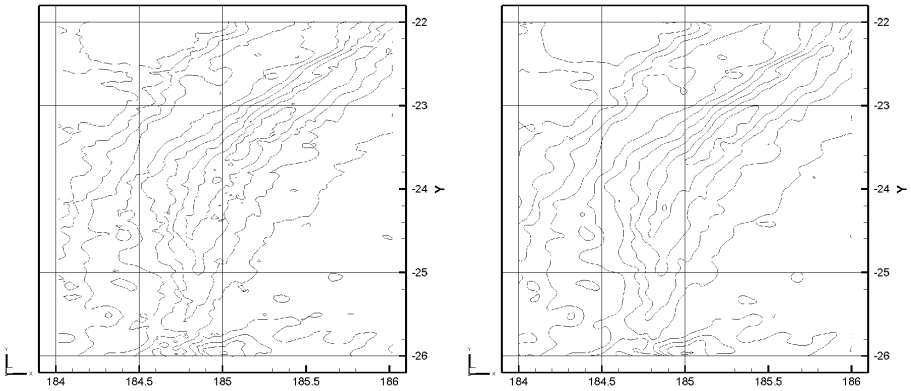

Figure 18: Left: Contour plot of the South Tonga Trench dataset. Right: Contour plot of the South Tonga Trench approximant.

6.3 Geological surface with fault

In this section we give another example based on real data values which come from the Vallée d'Ossau, Pyrénées mountains, France.

The Ground Penetrating Radar (GPR) technique is based on the principle that high-frequency electromagnetic waves may be reflected at boundaries separating heterogeneous regions of the subsurface. This technique is a very high resolution geophysical tool, with a penetration depth of a few tens of meters (100 m in the best conditions), depending on the underground physical properties and on the radar wave frequency used. Usually, GPR surveys are conducted with a constant offset between transmitter and receiver and a single-fold coverage. The time unit is the nanosecond, the frequency range is between 10 MHz and 1 GHz. The propagation velocity range is between 0.01 and 0.3m/ns, for example 0.12m/ns in limestone, 0.07m/ns in silts. In this study, we have used a frequency of 100 MHz, an offset of 1m and we have obtained a penetration depth of about 10m.

The studied area is located in the Western Pyrénées (30 km south of Pau, Béarn, France) in the Vallée d'Ossau which is an old glacial valley. 2D experiments were conducted and gave information on the sub-surface structures in the area. The interface between the limestone bedrock and the fluvio-glacial deposits has a depth varying between 2-3 meters and 12-13 meters with a weak general dip from the north to the south (about 2 degrees). Above this interface, the fluvio-glacial deposits show several sedimentary figures, with meter or decameter scale, which could correspond to old fluvial channels. However, this 2D acquisition cannot give us enough information to precisely describe the structures present on the site. The solution was to conduct a 3D GPR experiment on a part of the area, in order to obtain 3D information. So, a 3D GPR data acquisition on the area described above has been conducted. The single-fold GPR data were acquired along north-south profiles. The acquisition area corresponds to a rectangle of 38m $\times$ 35m. Throughout the whole acquisition work, a constant distance of 1m was maintained between the transmitter and receiver antennae, and both antennae were oriented perpendicular to the profile direction. Each trace was vertically stacked 256 times in the field. The sampling rate was 0.676ns and the trace length 300ns.

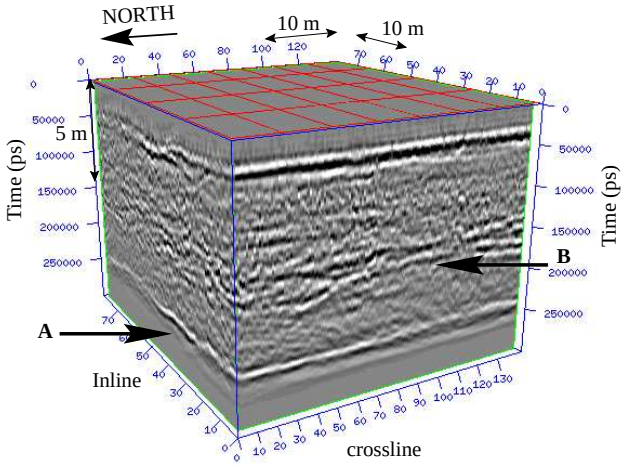

Figure 19: View of the 3D data block. A and B correspond to 2 horizons. In this work we will use the dataset corresponding to Horizon A.

Figure 19 shows the 3D view of the cuboid. Continuity of reflectors is better in the inline direction because the number of traces is higher (141 for inline instead of 77 for crossline sections). A strong and continuous reflector (called Horizon A) appears at about 250ns and is present on all the traces. According to the field observations and the first interpretation with the 2D profiles, this lowermost reflector can be interpreted as the interface between the limestone bedrock and the fluvio-glacial deposits.

In order to test our algorithm, we have modified the dataset to create a fault. 2D and 3D views of the considered dataset are given in Figures 20(left) and 21 respectively.
Here are the parameters used when running the proposed algorithm on this second real world example:

- the triangulation is made using 400 triangles;
- the finite element adopted is the Argyris triangle (class C^1);
- the smoothing parameter ϵ is chosen equal to 10^{-6};
- the evaluation grid is 150×150.

The quadratic error on the 8949 data points turns out to be equal to $2.332\ 10^{-3}$. The obtained approximant is depicted in Figures 20(right) and 22 where a 2D and a 3D view are given respectively. As it appears, no oscillations are present and excellent reconstruction results can be achieved.

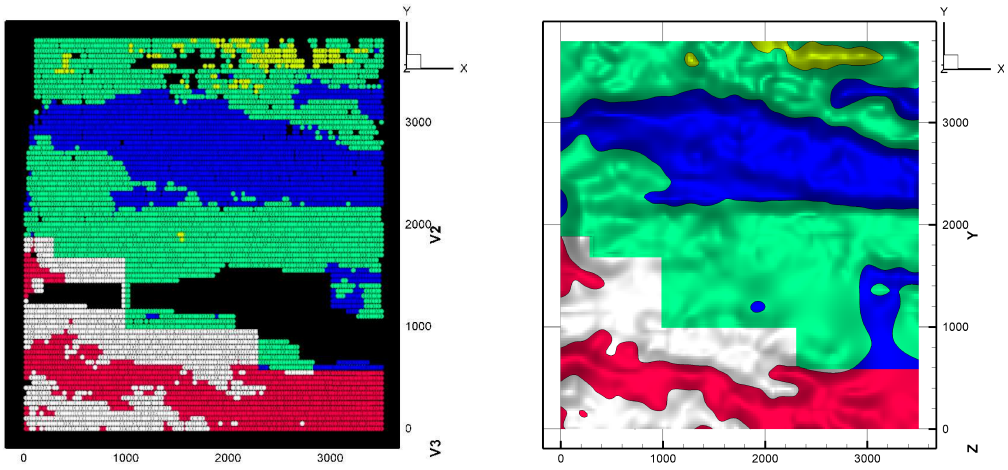

Figure 20: Left: 2D view of the geological dataset (8949 data points) containing a fault in correspondence to the boundaries with the white regions. Right: 2D view of the locally C^1 approximant of the geological surface with the fault.

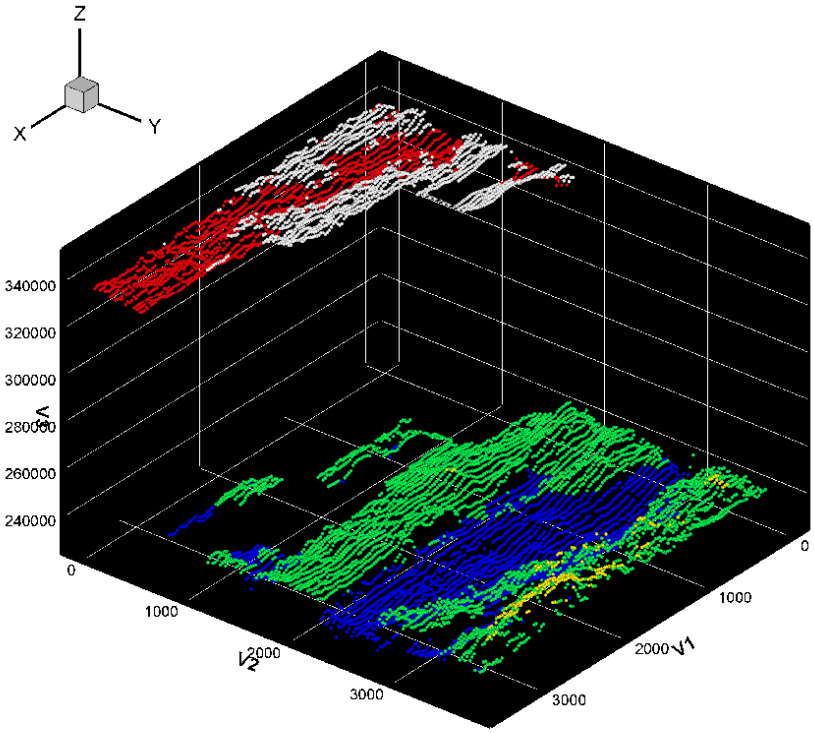

Figure 21: 3D view of the dataset corresponding to the geological surface with the fault (8949 data points).

7 Conclusions

In this paper, we have developed a novel and efficient algorithm for approximating non regular gridded data exhibiting large and rapid variations and/or complex fault structures.

The main steps of the proposed strategy consist in (i) accomplishing a pre-processing phase to define the set of discontinuities of the surface, (ii) generating a triangular mesh taking into account these discontinuities, (iii) applying a specific (known) finite element domain decomposition method and using a spline operator that relies on scale transformations (which seems to be very useful in controlling the behavior of the surface in the presence of steep gradients not found by the segmentation process) to

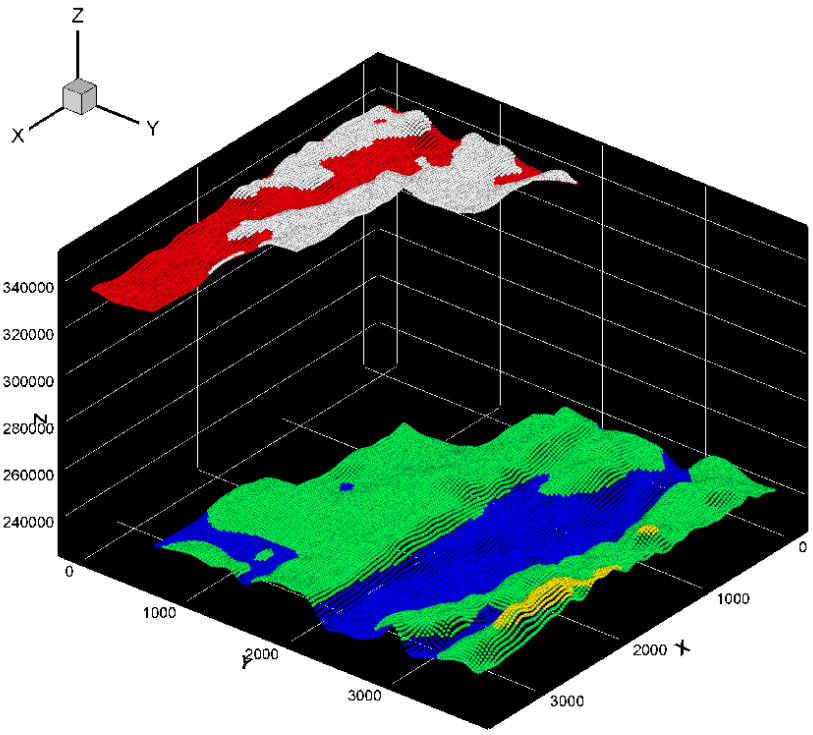

Figure 22: 3D view of the locally C^1 approximant of the geological surface with the fault. The approximant has been evaluated on an evenly space grid made of 150×150 points. The same scale and colormap are used for each surface. The general agreement is excellent. No oscillations are present.

produce the final approximating surface. Compared with conventional data fitting methods that exist in the literature, the proposed algorithm is able to suppress or at least decrease the undesired oscillations that generally arise near steep gradients, thus ensuring a faithful and accurate representation. The presented numerical examples illustrate the efficacy of the method.
Future research will be addressed towards an improvement of the meshing construction in order to make the algorithm fully automatic at each step. Moreover, future works will also focus on improving the segmentation process in order to guarantee more accurate results in the case of scattered datasets, without making use of the Large Variation Algorithm phase.

Acknowledgements The authors are very grateful to the referees of Numerical Algorithms for their careful reading of the manuscript and for their comments which were very helpful in preparing the final and improved version of the paper.

References

[1] D. Apprato, C. Gout, A result about scale transformation families in approximation: application to surface fitting from rapidly varying data, Numerical Algorithms 23 (2,3), 263-279, 2000.

[2] D. Apprato, R. Arcangéli, R. Manzanilla, Sur la construction de surfaces de classe C^k à partir d' un grand nombre de données de Lagrange, M^2AN, 21 (4), 529-555, 1987.

[3] D. Apprato, C. Gout and P. Sénéchal, C^k reconstruction of surfaces from partial data, Mathematical Geology 32 (8), 969-983, 2000.

[4] D. Apprato, C. Gout and D. Komatitsch, A new method for C^k approximation from a set of curves: application to ship track data in the Marianas trench, Mathematical Geology 34(7), 831-843, 2002.

[5] R. Arcangéli, Some application of discrete D^m-spline, Math. Methods in CAGD, T. Lyche and L.L. Schumaker eds., Academic Press, 35-44, 1989.

[6] R. Arcangéli, R. Manzanilla, J.J. Torrens, Approximation spline de surfaces de type explicite comportant des failles, Math. Model. and Num. Anal. 31 (5), 643-676, 1997.

[7] R. Arcangéli, M.C. Lopez de Silanes and J.J. Torrens, Multidimensional minimizing splines. Theory and applications. Kluwer Academic Publishers, Boston, MA, (ISBN: 1-4020-7786-6), 2004.

[8] R. Arcangeli, and J. L. Gout, Error estimates for Lagrange interpolation - Sur l'evaluation de l'erreur d'interpolation de Lagrange dans un ouvert de R^n, Math. Model. and Num. Anal., RAIRO Anal. Numer. 10(3), 5–27, 1976.

[9] G. Awanou, M. J. Lai, and P. Wenston, The multivariate spline method for scattered data fitting and numerical solution of partial differential equations, in Wavelets and Splines: Athens 2005, G. Chen and M. J. Lai (eds.), Nashboro Press, 24-74, 2006.

[10] C. de Boor, A Practical Guide to Splines, Springer Verlag, Berlin-Heidelberg, 1978.

[11] A. Bouhamidi, A. Le Méhauté, Multivariate interpolating (m, l, s)-splines, Adv. in Comput. Math. 11 (4), 287-314, 1999.

[12] M. Bozzini, L. Lenarduzzi, Recovering a Function with Discontinuities from Correlated Data, in Advanced Topics in Multivariate Approximation, F. Fontanella, K. Jetter and P.J. Laurent (eds.), WSP Singapore, 1996.

[13] M. Bozzini, M. Rossini, Approximating surfaces with discontinuities, Mathematical and Computer Modelling 31 (6/7), 193-216, 2000.

[14] G. Casciola, E. Franchini and L. Romani, The mixed directional difference-summation algorithm for generating the Bézier net of a trivariate four-direction Box-spline. Numerical Algorithms 43 (1), 75-98, 2006.

[15] V. Caselles, R. Kimmel, G. Sapiro, Geodesic Active Contours, Geodesic Active Contours, International Journal of computer Vision 22-1, 61-87, 1997.

[16] A. Chakraborty, L. Staib, and J. Duncan, Deformable boundary finding in medical images by integrating gradient and region information, IEEE Trans. Medical Imaging 15-6, p. 859-870, 1996.

[17] P.G. Ciarlet, The finite element method for elliptic problems, North Holland, 1977.

[18] L.N. Deshpande, D.A. Girard, Fast computation of cross-validation robust splines and other nonlinear smoothing splines, in Curves and Surfaces, Academic Press, 143-148, 1991

[19] T.A. Foley, Weighted bicubic spline interpolation to rapidly varying data, ACM Trans. Graphics 6, 1-18, 1987.

[20] R. Franke, Smooth interpolation of scattered data by local thin plate splines, Comp & Maths with Appls. 8 (4), 273-281, 1982.

[21] GAMMA meshing, INRIA, http://www-c.inria.fr/gamma/download/.

[22] D.A. Girard, Monte-Carlo cross-validation procedure for large least squares problems with noisy data, Numer. Math. 56-1, 1-23, 1989.

[23] C. Gout and C. Le Guyader, Segmentation of complex geophysical structures with well data. Comput. Geosci. 10 (4), 361-372, 2006.

[24] C. Gout and D. Komatitsch, Surface fitting of rapidly varying data using rank coding: application to geophysical surfaces, Mathematical Geology 32 (7), 873-888, 2000.

[25] C. Gout, C. Le Guyader and L. Vese, Segmentation under geometrical conditions using geodesic active contours and interpolation using level set methods, Numerical Algorithms 39 (1,3), 155-173, 2005.

[26] J.L. Gout, Error estimates for Hermite interpolation - Estimation de l'erreur d'interpolation d'Hermite dans R^n. [French] Numer. Math. 28, no. 4, 407–429, 1977.

[27] T. Gutzmer, A. Iske, Detection of discontinuities in scattered data approximation, Numerical Algorithms 16(2), 155-170, 1997.

[28] C. Le Guyader, D.Apprato and C. Gout, Using a Level Set Approach for Image segmentation under interpolation conditions, Numerical Algorithms 39 (1-3), 221-235, 2005.

[29] P.J. Laurent, Approximation et optimisation, Hermann, Paris, 1972.

[30] R. Malladi, J.A. Sethian, Image processing via level set curvature flow, Proceedings of the National Academy of Sciences, vol. 92 (15), 7046-7050, 1995.

[31] R. Malladi, J.A. Sethian and B.C. Vemuri, in: A fast level set based algorithm for topology independent shape modeling and recovery, Proc. of the third ECCV, Stockholm, Sweden, 3-13, 1994.

[32] R. Manzanilla, Sur l'approximation de surfaces définies par une équation explicite, Thèse, Université de Pau, 1986.

[33] MEFISTO, A. Perronet, http://www.ann.jussieu.fr/~perronnet/mefisto.charger.php3

[34] METIS, METIS - Serial Graph Partitioning and Fill-reducing Matrix Ordering, download at URL: http://glaros.dtc.umn.edu/gkhome/views/metis

[35] J. Nečas, Les méthodes directes en théorie des équations elliptiques, Masson, Paris 1967.

[36] G. M. Nielson and R. Franke, A method for construction of surfaces under tension, Rocky Mountain J. Math. 14, 203-221, 1984.

[37] S. Osher and J.A. Sethian, Fronts propagation with curvature dependant speed: Algorithms based on Hamilton-Jacobi formulations, Journal of Computational Physics 79, 12-49, 1988.

[38] S. Osher and R. Fedkiw, Level Set Methods and Dynamic Implicit Surfaces (Springer Verlag, 2003).

[39] N. Paragios and R. Deriche, Geodesic Active Regions for Supervised Texture Segmentation, Proceedings of ICCV, 1999.

[40] M.C. Parra, M.C. Lopez de Silanes and J.J Torrens, Vertical Fault Detection from Scattered Data, Journal of Computational and Applied Mathematics 73(5), 225-239, 1996.

[41] L. Romani and M.A. Sabin, The conversion matrix between uniform B-spline and Bézier representations. Comput. Aided Geom. Design 21 (6), 549-560, 2004.

[42] R. Ronfard, Region-based strategies for active contour models, Int. J. Computer Vision 13-2, p. 229-251, 1994.

[43] K. Salkauskas, C^1splines for interpolation of rapidly varying data, Rocky Mountain J. Math. 14, 239-250, 1974.

[44] C. Samson, L. Blanc-Feraud, G. Aubert, and J. Zerubia, A level set method for image classification, Int. Conf. Scale-Space Theories in Computer Vision, p. 306-317, 1999.

[45] I.J. Schoenberg, Contribution to the problem of approximation of equidistant data by anlytic functions, Quart. of Appl. Math. 4, 45-99 and 112-141, 1960.

[46] L.L. Schumaker, Fitting surfaces to scattered data, in Approximation Théorie II, G.G. Lorentz, C.K. Chui et L.L. Schumaker (éditeurs), Academic Press, 203-269, 1976.

[47] L.L. Schumaker and M. von Golitschek, Penalized least squares fitting, Serdica 18 (2002), 1001–1020.

[48] J.A. Sethian, Level Set Methods and Fast Marching Methods: Evolving interfaces in Computational Geometry, Fluid Mechanics, Computer Vision and Material Science, second edition, Cambridge University Press, 378 p., 1999

[49] J.J. Torrens, Interpolacion de superficies parametricas con discontinuidades mediante, Elementos Finitos, Aplicaciones, Thèse, Universidad de Zaragoza, Spain, 1991.

[50] L. A. Vese, T. F. Chan, A Multiphase Level Set Framework for Image Segmentation Using the Mumford and Shah Model, International Journal of Computer Vision, 50 (3), 271-293, 2002.

[51] A. Zenisek, A General Theorem on Triangular Finite C^m - Elements, RAIRO R-2, 119-127, 1974.